

Bayesian phase difference estimation based on single-photon projective measurement

Xu-Hao Yu(余旭豪), Ying Wei(韦颖), Ran Yang(杨然), Wen-Hui Song(宋文慧), Yingning Miao(缪应宁), Wei Zhou(周唯), Xinhui Li(李新慧), Xiaoqin Gao(高小钦), Yan-Xiao Gong(龚彦晓), and Shi-Ning Zhu(祝世宁)
Citation: Chin. Phys. B, 2025, 34 (**7**): 070305. DOI: 10.1088/1674-1056/adde33
Journal homepage: http://cpb.iphy.ac.cn; http://iopscience.iop.org/cpb

What follows is a list of articles you may be interested in

Quantum-enhanced time-of-arrival measuring method based on partially entangled state

Peng-Xian Li(李芃鲜), Lu-Ping Xu(许录平), Gui-Ting Hu(胡桂廷), Wen-Long Gao(高文珑)
Chin. Phys. B, 2025, 34 (**7**): 070303. DOI: 10.1088/1674-1056/adc7ee

Precision bounds for quantum phase estimation using two-mode squeezed Gaussian states

Jian-Dong Zhang(张建东), Chuang Li(李闯), Lili Hou(侯丽丽), and Shuai Wang(王帅)
Chin. Phys. B, 2025, 34 (**1**): 010304. DOI: 10.1088/1674-1056/ad8dc0

Enhanced measurement precision with continuous interrogation during dynamical decoupling

Jun Zhang(张军), Peng Du(杜鹏), Lei Jing(敬雷), Peng Xu(徐鹏), Li You(尤力), and Wenxian Zhang(张文献)
Chin. Phys. B, 2024, 33 (**3**): 030301. DOI: 10.1088/1674-1056/ad1985

Tolerance-enhanced SU(1,1) interferometers using asymmetric gain

Jian-Dong Zhang(张建东) and Shuai Wang(王帅)
Chin. Phys. B, 2023, 32 (**1**): 010306. DOI: 10.1088/1674-1056/ac981d

Quantum metrology with coherent superposition of two different coded channels

Dong Xie(谢东), Chunling Xu(徐春玲), and Anmin Wang(王安民)
Chin. Phys. B, 2021, 30 (**9**): 090304. DOI: 10.1088/1674-1056/ac0bae

---

RAPID COMMUNICATION

Bayesian phase difference estimation based on single-photon projective measurement

Xu-Hao Yu(余旭豪)[†], Ying Wei(韦颖)[†], Ran Yang(杨然), Wen-Hui Song(宋文慧), Yingning Miao(缪应宁), Wei Zhou(周唯), Xinhui Li(李新慧), Xiaoqin Gao(高小钦), Yan-Xiao Gong(龚彦晓)[‡], and Shi-Ning Zhu(祝世宁)

National Laboratory of Solid State Microstructures, School of Physics, Jiangsu Physical Science Research Center, and Collaborative Innovation Center of Advanced Microstructure, Nanjing University, Nanjing 210093, *China*

(Received 5 May 2025; revised manuscript received 29 May 2025; accepted manuscript online 29 May 2025)

The estimation of quantum phase differences plays an important role in quantum simulation and quantum computation, yet existing quantum phase estimation algorithms face critical limitations in noisy intermediate-scale quantum (NISQ) devices due to their excessive depth and circuit complexity. We demonstrate a high-precision phase difference estimation protocol based on the Bayesian phase difference estimation algorithm and single-photon projective measurement. The iterative framework of the algorithm, combined with the independence from controlled unitary operations, inherently mitigates circuit depth and complexity limitations. Through an experimental realization on the photonic system, we demonstrate high-precision estimation of diverse phase differences, showing root-mean-square errors (RMSE) below the standard quantum limit $\mathcal{O}(1/\sqrt{N})$ and reaching the Heisenberg scaling $\mathcal{O}(1/N)$ after a certain number of iterations. Our scheme provides a critical advantage in quantum resource-constrained scenarios, and advances practical implementations of quantum information tasks under realistic hardware constraints.

Keywords: Bayesian phase difference estimation, single-photon projection measurement, Heisenberg limit, quantum information, quantum state engineering and measurements

PACS: 03.67.Lx, 03.67.Ac, 42.50.Dv, 03.67.Ac

DOI: 10.1088/1674-1056/adde33 **CSTR:** 32038.14.CPB.adde33

1. Introduction

The estimation of quantum phase differences has vital applications in quantum metrology,[1–3] quantum simulation,[4–6] quantum chemistry,[7,8] and quantum computing,[9–14] enabling precise determination of molecular and atomic energy gaps,[15,16] spectral analysis,[17] chemical reaction rate prediction.[18] However, conventional quantum phase estimation (QPE) faces critical limitations in the noisy intermediate-scale quantum (NISQ) era. Specifically, its dependence on a large number of ancillary qubits[19] and deep quantum circuits makes it highly susceptible to errors, rendering it impractical under current quantum resource constraints.[20] To address these challenges, hybrid quantum-classical algorithms have been developed, such as iterative quantum phase estimation (IQPE) and Bayesian phase estimation (BPE).[21–25] These algorithms utilize just one ancillary qubit, decomposing complex circuits into iterative shallow subroutines, thus reducing circuit depth and enhancing their compatibility with NISQ devices. However, both IQPE and BPE require controlled unitary operations,[26,27] a requirement that inherently increases quantum circuit complexity and consequently compromises experimental feasibility. In contrast, the Bayesian phase difference estimation (BPDE) algorithm[28] circumvents the need for controlled unitary operations, and instead only requires state preparation (controlled-Excite) and its inverse. Notably, controlled-Excite gates exhibit shallower circuit depths than the controlled unitary operations required by IQPE and BPE, positioning BPDE as a resource-efficient and NISQ-implementable solution.

In this work, we experimentally implement a BPDE algorithm on the photonic quantum system and achieve high-precision estimation of phase difference values. Unlike conventional phase estimation algorithms that employ majority voting schemes,[29,30] our approach constructs the likelihood function from single-photon projective measurement results. We estimate three types of phase difference values, including small, randomized, and special phases, demonstrating root-mean-square errors (RMSE) below the standard quantum limit $\mathcal{O}(1/\sqrt{N})$ and reaching Heisenberg-limited scaling $\mathcal{O}(1/N)$.[31–34] The universality of the algorithm for arbitrary unknown phases, combined with its use of single-photon projective measurements, establishes a resource-efficient framework for quantum information processing in resource-constrained NISQ environments.

[†]These authors contributed equally to this work.

[‡]Corresponding author. E-mail: gongyanxiao@nju.edu.cn

© 2025 Chinese Physical Society and IOP Publishing Ltd. All rights, including for text and data mining, AI training, and similar technologies, are reserved.

2. Bayesian phase difference estimation

We consider that an evolution unitary operator $\hat{U}$ corresponding to an underlying Hamiltonian has two eigenstates $|\psi_0\rangle$ and $|\psi_1\rangle$, such that

$$\hat{U}|\psi_k\rangle = \mathrm{e}^{\mathrm{i}\alpha_k}|\psi_k\rangle, \tag{1}$$

where $k = 0$ and 1 represent the ground and the excited states, respectively. The eigenphase difference $\phi = \alpha_1 - \alpha_0$ is the unknown phase to be estimated, and we assume $\phi \in [0, 2\pi)$.

The quantum circuit for BPDE is shown in Fig. 1(a). Initially, an ancillary qubit is in state $|0\rangle_\mathrm{C}$ and the system state is in the eigenstate $|\psi_0\rangle_\mathrm{S}$, with the subscripts C and S denoting control qubit and system, respectively. After the Hadamard gate $\hat{H}_\mathrm{C}$ the control qubit evolves into $(|0\rangle_\mathrm{C} + |1\rangle_\mathrm{C})/\sqrt{2}$. Then, a controlled-Excite operation $\hat{U}_\mathrm{C\text{-}E}$ is introduced with the ancillary and system states acting as the control and target qubits, respectively. Explicitly, the operation can be expressed as $\hat{U}_\mathrm{C\text{-}E} = |0\rangle_\mathrm{C}\langle 0|_\mathrm{C} \otimes \hat{I}_\mathrm{S} + |1\rangle_\mathrm{C}\langle 1|_\mathrm{C} \otimes \hat{E}_\mathrm{S}$, where the excitation operator $\hat{E}_\mathrm{S}|\psi_0\rangle_\mathrm{S} = |\psi_1\rangle_\mathrm{S}$. Hence, after the controlled-Excite operation, the two-qubit state becomes $(|0\rangle_\mathrm{C}|\psi_0\rangle_\mathrm{S} + |1\rangle_\mathrm{C}|\psi_1\rangle_\mathrm{S})/\sqrt{2}$. Next, the unitary operation U given in Eq. (1) is applied to the system state M times, and consequently, the two-qubit state transforms into $\mathrm{e}^{\mathrm{i}M\alpha_0}(|0\rangle_\mathrm{C}|\psi_0\rangle_\mathrm{S} + \mathrm{e}^{\mathrm{i}M\phi}|1\rangle_\mathrm{C}|\psi_1\rangle_\mathrm{S})/\sqrt{2}$. Then, a controlled-inverse-Excite operation is implemented, expressed as $\hat{U}_\mathrm{C\text{-}IE} = |0\rangle_\mathrm{C}\langle 0|_\mathrm{C} \otimes \hat{I}_\mathrm{S} + |1\rangle_\mathrm{C}\langle 1|_\mathrm{C} \otimes \hat{E}_\mathrm{S}^\dagger$, where $\hat{E}_\mathrm{S}^\dagger|\psi_1\rangle_\mathrm{S} = |\psi_0\rangle_\mathrm{S}$. Hence, the two-qubit state evolves into $\mathrm{e}^{\mathrm{i}M\alpha_0}(|0\rangle_\mathrm{C} + \mathrm{e}^{\mathrm{i}M\phi}|1\rangle_\mathrm{C})|\psi_0\rangle_\mathrm{S}/\sqrt{2}$. Next, a phase shift gate with a parameter $\Delta\varepsilon$ for estimation is performed on the control qubit, given by

$$\hat{T}_\mathrm{C}(-M\Delta\varepsilon) = |0\rangle_\mathrm{C}\langle 0|_\mathrm{C} + \mathrm{e}^{-\mathrm{i}M\Delta\varepsilon}|1\rangle_\mathrm{C}\langle 1|_\mathrm{C}. \tag{2}$$

Finally, after a Hadamard gate $\hat{H}_\mathrm{C}$ on the control qubit, the two-qubit state evolves into

$$\begin{aligned}&\frac{1}{2}\mathrm{e}^{\mathrm{i}M\alpha_0}\{[(1+\mathrm{e}^{\mathrm{i}M(\phi-\Delta\varepsilon)}]|0\rangle_\mathrm{C}\\&+[1-\mathrm{e}^{\mathrm{i}M(\phi-\Delta\varepsilon)}]|1\rangle_\mathrm{C}\}|\psi_0\rangle_\mathrm{S}.\end{aligned} \tag{3}$$

Hence, the measurement probabilities of projecting the ancillary qubit on state $|0\rangle_\mathrm{C}$ and $|1\rangle_\mathrm{C}$ are respectively given by

$$P(r=0) = \frac{1}{2}\{1+\cos[M(\phi-\Delta\varepsilon)]\}, \tag{4}$$

$$P(r=1) = \frac{1}{2}\{1-\cos[M(\phi-\Delta\varepsilon)]\}, \tag{5}$$

where $r \in \{0,\ 1\}$ denotes the measurement outcome.

To simplify the phase estimation process, we diagonalize the unitary operator $\hat{U}_\mathrm{S}$ in the basis $\{|\psi_0\rangle,\ |\psi_1\rangle\}$, and define $|0\rangle_\mathrm{S} \equiv |\psi_0\rangle$ and $|1\rangle_\mathrm{S} \equiv |\psi_1\rangle$, having

$$\begin{aligned}\hat{U}_\mathrm{S} &= \mathrm{e}^{\mathrm{i}\alpha_0}|0\rangle_\mathrm{S}\langle 0|_\mathrm{S} + \mathrm{e}^{\mathrm{i}\alpha_1}|1\rangle_\mathrm{S}\langle 1|_\mathrm{S}\\&= \mathrm{e}^{\mathrm{i}\alpha_0}\left(|0\rangle_\mathrm{S}\langle 0|_\mathrm{S} + \mathrm{e}^{\mathrm{i}\phi}|1\rangle_\mathrm{S}\langle 1|_\mathrm{S}\right).\end{aligned} \tag{6}$$

In this case, the excitation operation $\hat{E}_\mathrm{S}$ and its inverse can be written as the NOT gate $\hat{X}_\mathrm{S}$, and consequently, the controlled-Excite and controlled-inverse-Excite operations are both equivalent to the C-NOT operation, as shown in Fig. 1(b).

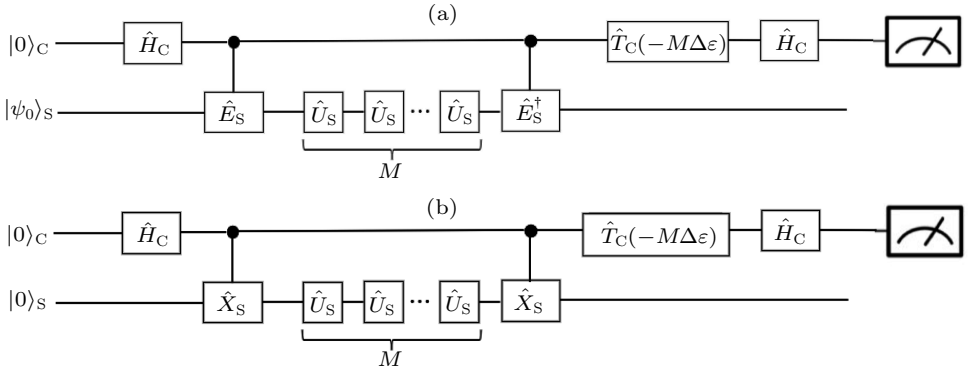


Fig. 1. The quantum circuit diagram for Bayesian phase difference estimation of (a) a general unitary operator and (b) the diagonalized unitary operator.

Beyond the quantum circuit in Fig. 1, the BPDE further utilizes classical algorithms to process quantum measurement results to obtain the posterior distribution and update the parameters of the circuit for subsequent iterations. In contrast to the traditional BPE algorithm, we adopt the rejection filtering phase estimation (RFPE) algorithm.[27] In this regard, a prior Gaussian probability distribution $P(\phi) = \mathcal{N}(\mu,\ \sigma^2)$ is used to represent the confidence that the current hypothesis aligns with the true phase ϕ. The likelihood function is determined by the projection measurement probabilities given by Eqs. (4) and (5), namely, $P(r|\phi;\Delta\varepsilon,M) = P(r)$. According to the Bayesian inference, after the measurement result, the posterior probability distribution of ϕ is

$$P(\phi|r;\Delta\varepsilon,M) = \frac{P(r|\phi;\Delta\varepsilon,\ M)P(\phi)}{\int P(r|\phi;\Delta\varepsilon,M)P(\phi)\,\mathrm{d}\phi}. \tag{7}$$

The detailed procedure is outlined as follows.

I. Set an initial normal distribution $\mathcal{N}_0(\mu_0,\sigma_0^2)$, which is taken as the initial prior distribution $\mathcal{N}_1(\mu_1,\sigma_1^2)$.

II. Based on the prior distribution $\mathcal{N}_1$, parameters M and $\Delta\varepsilon$ are determined by $M = \lceil 1.25/\sigma_1 \rceil$, and $\Delta\varepsilon = \mu_1$, respectively, where $\lceil\cdot\rceil$ means taking an upward integer. The parameters are applied to the quantum circuit to obtain the projection measurement outcome $r \in \{0,1\}$.

III. Through a classical computer, $m = 1000$ samples $\{x_i\}$ are randomly selected according to the prior distribution $\mathcal{N}_1$.

IV. From Eqs. (4) and (5), the likelihood function corresponding to the outcome r is constructed as $P(0|x_i;\Delta\varepsilon,M) = \{1+\cos[M(x_i-\Delta\varepsilon)]\}/2$ and $P(1|x_i;\Delta\varepsilon,M) = \{1-\cos[M(x_i-\Delta\varepsilon)]\}/2$. Then with these probabilities the accepted samples $\{x_{\text{accept}}\}$ are generated, which satisfy the posterior distribution as well according to Eq. (7).

V. The mean μ_2 and standard deviation σ_2 of the accepted samples $\{x_{\text{accept}}\}$ are calculated to obtain the posterior distribution $\mathcal{N}_2(\mu_2,\sigma_2^2)$.

VI. Determine if the convergence condition has been met. If not, set the posterior distribution $\mathcal{N}_2$ as the new prior distribution $\mathcal{N}_1$, and then repeat steps II through V. Once the convergence condition is satisfied, terminate the iteration process.

3. Experimental setup

In our experiment, we demonstrate the BPDE algorithm shown in Fig. 1(b) for high-precision estimation of phase differences in the photonic quantum system. The experimental setup is shown in Fig. 2. A 2-cm-long periodically-poled potassium titanyl phosphate (PPKTP) crystal is pumped by a continuous-wave laser (MDL-E-405-50 mW FI91719) with wavelength of 405.6 nm to produce non-degenerate photon pairs at 809 nm and 813.4 nm through the type-II spontaneous parametric down-conversion (SPDC) process. The polarization state of the pump laser is controlled by the half-wave plate (HWP) H_p and the quarter-wave plate (QWP) Q_p. The orthogonally polarized photon pairs are separated at the polarizing beam splitter PBS_1, where the vertically polarized idler photons are reflected and then detected through a single-photon detector (SPD_1) to serve as the trigger, while the horizontally polarized signal photons are transmitted to the quantum circuit for BPDE.

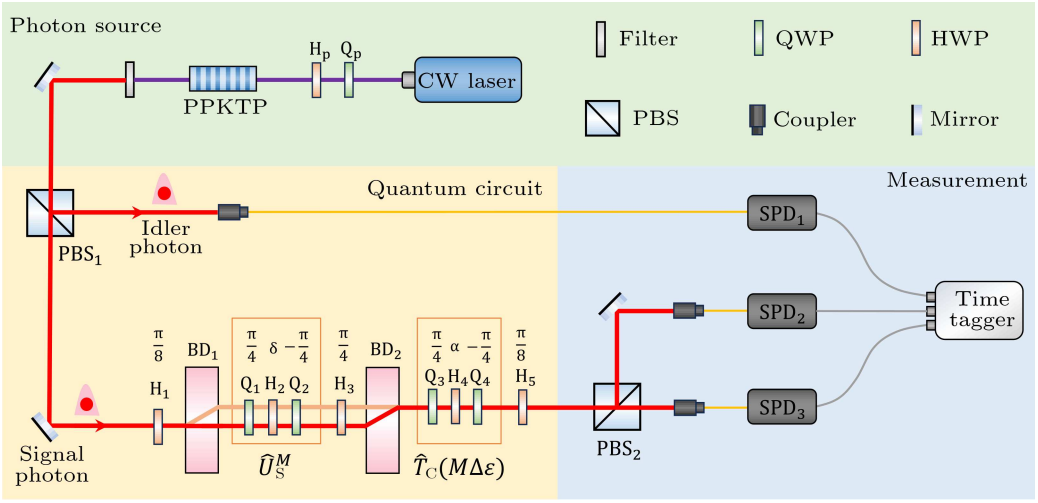


Fig. 2. Experimental setup for BPDE. PPKTP: periodically-poled potassium titanyl phosphate; QWP: quarter-wave plate; HWP: half-wave plate; PBS, polarizing beam splitter; BD: beam displacer; SPD: single-photon detector.

The signal photons then pass through the HWP H_1 oriented at 22.5°, which acts as the Hadamard gate on the polarization qubit, the control qubit, with the definition of $|0\rangle_C \equiv |H\rangle$, $|1\rangle_C \equiv |V\rangle$. Next, the beam displacer BD_1 displaces the horizontally polarized photons by 2.8 mm. We define the displaced upper and lower paths as the system qubit states $|0\rangle_S$ and $|1\rangle_S$, respectively. Then we employ a combination of QWP–HWP–QWP lying in both paths to implement the M times diagonalized unitary operation $\hat{U}_S^M$, where the axes of Q_1 and Q_2 are set to 45° and −45°, respectively, and the axis angle of H_2, δ, is related to the phase shift value by $\delta = M\phi/4$. Note that, although the phase shift is between the horizontal and vertical polarizations, we get an equivalent phase shift operation on the path qubits, as photons in the upper and lower paths are horizontally and vertically polarized, respectively. Hence, the two-qubit state evolves into $(|0\rangle_C|0\rangle_S + e^{iM\phi}|1\rangle_C|1\rangle_S)/\sqrt{2}$, where the global phase is omitted. It should be noted that, while the protocol in Fig. 1 requires M repetitions of an unknown phase shift operation, our experimental implementation employs a tunable phase shift configuration to simulate these sequential operations for proof-of-principle demonstration. Subsequently, photons in both paths pass through the HWP H_3 oriented at 45° to reverse their polarization states, and are then combined into one path at the beam displacer BD_2. Thereafter, the phase shift operation $\hat{T}_C(M\Delta\varepsilon)$ is likewise realized through the combination of QWP–HWP–QWP composed of Q_3, H_4, Q_4, with the axis angle of H_4 $\alpha = M\Delta\varepsilon/4$. Following this, the HWP H_5 oriented at 22.5° performs the Hadamard gate on the polarization qubit. Conse-

quently, we can write the final state as

$$\frac{1}{2}\left\{\left[1+\mathrm{e}^{\mathrm{i}M(\Delta\varepsilon-\phi)}\right]|0\rangle_{\mathrm{C}}+\left[1-\mathrm{e}^{\mathrm{i}M(\Delta\varepsilon-\phi)}\right]|1\rangle_{\mathrm{C}}\right\}|0\rangle_{\mathrm{S}}. \quad (8)$$

In the measurement part, the vertically and horizontally polarized photons are separated at the polarizing beam splitter PBS_2 and coupled into single-photon detectors SPD_2 and SPD_3, respectively. The coincidence counts of SPD_1 and SPD_2, C_1, and the coincidence counts of SPD_1 and SPD_3, C_2, are the results of the projection measurement in $|1\rangle_{\mathrm{C}}$ and $|0\rangle_{\mathrm{C}}$, respectively, with the corresponding projection probabilities given by Eqs. (4) and (5). Note that, to ensure the accuracy of the projection probability, we adjust the fiber coupling efficiency to ensure the same detection efficiency on SPD_2 and SPD_3. Moreover, as we employ the single-photon projective measurement, we appropriately reduce the pump power to maintain the coincidence count rate at approximately 1 Hz. Then we can estimate the true phase ϕ through $\Delta\varepsilon$ by adjusting δ and α, respectively. In the ideal case, when the estimated phase is equal to the true phase, namely, $\Delta\varepsilon-\phi=0$, we have $C_1=0$ and $C_2=1$.

4. Results and discussion

We begin by experimentally demonstrating the estimation of a small unknown phase, specifically targeting a true phase value set to $\phi_1=0.1^\circ\approx 1.745\times10^{-3}$ rad, to validate our protocol. The experimental results are shown in Fig. 3(a). We can see that after $n_1=98$ iterations, the estimated phase is obtained to be $\Delta\varepsilon_1=(1.74533\pm0.00038)\times10^{-3}$ rad, which aligns closely with the true phase. This agreement validates the effectiveness of BPDE in single-shot measurement scenarios. It should be noted that the experimental iteration is terminated once the convergence condition $\sigma/(\Delta\varepsilon)<10^{-3}$ is met. Furthermore, we analyze the root-mean-square errors (RMSE) from the estimated phase and the true phase. For an iteration number n, the RMSE with consumed resource number are expressed as $N=\sum_{i=1}^{n}M_i\mathbb{N}_i$, where $\mathbb{N}_i$ is the average number of photons used in each experimental iteration, and for the single-photon projection measurement, $\mathbb{N}_i=1$. As shown in Fig. 3(e), when the consumed resource number $N\geq60$ ($n\geq20$), the RMSE of the estimated phase are below the standard quantum limit. Moreover, the fitting curve of RMSE follows the Heisenberg scaling $\mathcal{O}(1/N)$. Hence, we achieve an accurate estimation on a small phase, and thus validate the superiority of BPDE. Note that since the phase to be estimated is completely unknown, the initial variance we select is relatively large, and the initial phase is also likely to be inconsistent with the true phase, so the convergence of RMSE in the early stage is relatively slow. Therefore, we mainly fit with data points in the range of $N>15$.

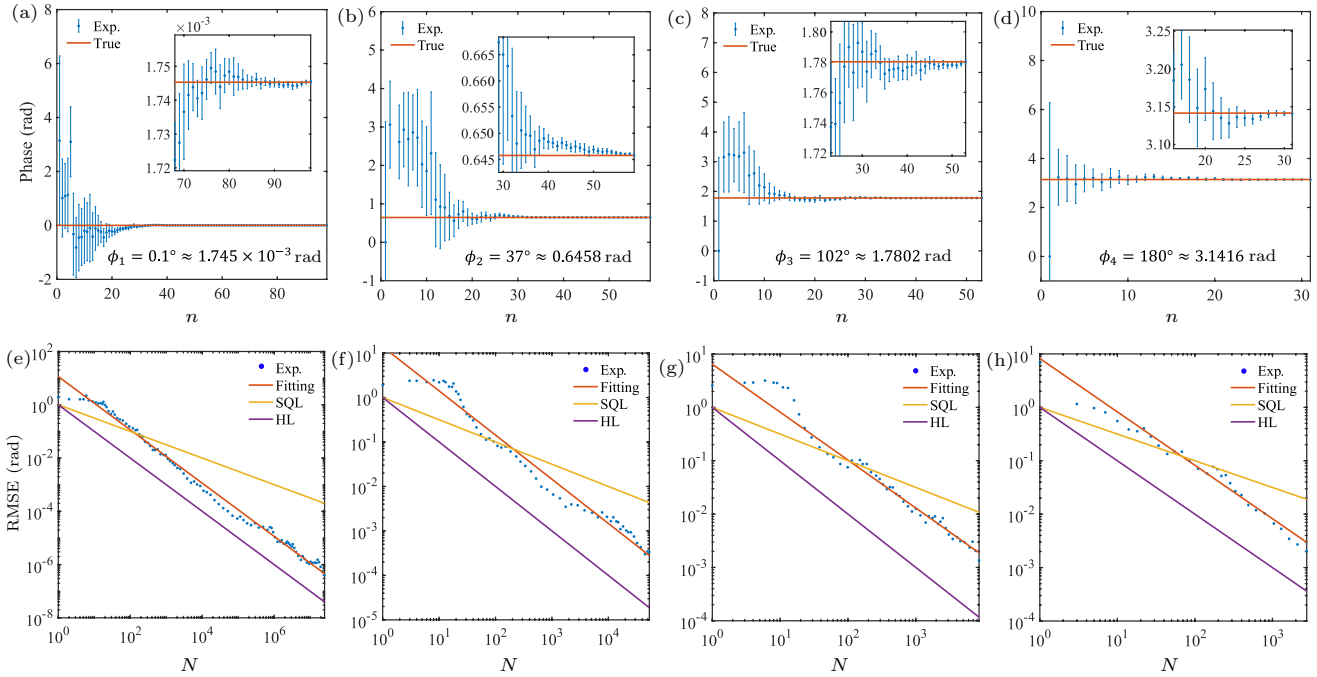


Fig. 3. Phase estimation process with different phase values. (a), (b), (c), and (d) are the estimated phases for $\phi_1=1.745\times10^{-3}$ rad, $\phi_2=0.6458$ rad, $\phi_3=1.7802$ rad, and $\phi_4=3.1416$ rad, respectively, with the corresponding RMSE plotted in (e), (f), (g), and (h). Here, n is the iteration number and N is the consumed resource number.

To verify the universality of the experimental scheme, we estimate several phase values, including $\phi_2=37^\circ\approx0.6458$ rad, $\phi_3=102^\circ\approx1.7802$ rad, and $\phi_4=180^\circ\approx3.1416$ rad, with the experimental results shown in Figs. 3(b), 3(c), and 3(d), respectively. Explicitly, we obtain the corresponding estimated phase values for the three true phases ϕ_2, ϕ_3, and ϕ_4 as $\Delta\varepsilon_2=0.64567\pm0.00033$ rad, $\Delta\varepsilon_3=1.7803\pm0.0013$ rad, and $\Delta\varepsilon_4=3.1411\pm0.0019$ rad, achieved with it-

erations $n_2 = 59$, $n_3 = 53$, and $n_4 = 31$, respectively. We can see that all of the estimated phase values are very close to the true phases. Furthermore, as shown in Figs. 3(e), 3(f), and 3(g), with $N > 100$, the RMSE are below the standard quantum limit and follow Heisenberg-limited scaling. These results demonstrate the universal applicability of our protocol for estimating any phase differences.

Finally, we examine potential errors that may arise from experimental imperfections, primarily due to the misalignment of waveplates. Before the experiment, all the waveplates were calibrated by using a PBS with an extinction ratio of 1000 : 1, and thus the errors of waveplate angles can be estimated to be $\pm 0.05^\circ$. The reading errors of the waveplate angles are approximately $\zeta = \pm 0.2^\circ$. Hence, the maximum deviation of the projection probability can be estimated to be 0.0034. Since the RFPE algorithm itself is robust to the projection error of at least $\zeta = \pm 0.1$, [27] its influence on the estimation results can be ignored.

5. Conclusion

In conclusion, we have presented an experimental demonstration of a high-precision phase difference estimation protocol in the photonic quantum system by employing the BPDE algorithm and single-photon projection measurements. The experimental results show that the root-mean-square errors (RMSE) surpass the standard quantum limit $\mathcal{O}(1/\sqrt{N})$ and reach the Heisenberg scaling $\mathcal{O}(1/N)$ after iterative optimization. The universality of our algorithm is validated through phase estimations across diverse parameter regimes, including small, randomized, and special phases. Crucially, compared to conventional schemes consuming a large number of photons, e.g., majority voting, our scheme requires only single-photon projective measurements in each experimental iteration, which offers significant advantages in quantum resource-constrained scenarios. Note that, although BPDE can split large-scale circuits through iteration, compared with the conventional quantum phase estimation, since BPDE needs to calculate the optimal number of operations M and the posterior distribution based on prior information and measurement results in each iteration, it consumes more classical computing resources. In addition, although the current implementation focuses on diagonalized unitary matrices, the methodology can be extended to arbitrary unitary operators. Our approach demonstrates a concrete framework for implementing quantum simulation protocols, for example, molecular energy gap calculations, on NISQ devices.

Acknowledgements

Project supported by the Natural Science Foundation of Jiangsu Province (Grant Nos. BK20233001 and BK20243060) and the National Natural Science Foundation of China (Grant No. 62288101).

References

[1] Zwierz M, Pérez-Delgado C A and Kok P 2010 *Phys. Rev. Lett.* **105** 180402
[2] Pezzè L, Smerzi A, Oberthaler M K, Schmied R and Treutlein P 2018 *Rev. Mod. Phys.* **90** 035005
[3] Reilly J T, Wilson J D, Jäger S B, Wilson C and Holland M J 2023 *Phys. Rev. Lett.* **131** 150802
[4] Aspuru-Guzik A, Dutoi A D, Love P J and Head-Gordon M 2005 *Science* **309** 1704
[5] Yang Y D, Li Y, Xu X S and Yuan X 2024 *Phys. Rev. A* **109** 052416
[6] Dong C X, Yang Z S, Zeng J F and Hu J P 2023 *Chin. Phys. B* **32** 070305
[7] Bauer B, Bravyi S, Motta M and Chan G K L 2020 *Chem. Rev.* **120** 12685
[8] Cao Y D, Romero J, Olson J P, *et al.* 2019 *Chem. Rev.* **119** 10856
[9] Peruzzo A, McClean J, Shadbolt P, Yung M H, Zhou X Q, Love P J, Aspuru-Guzik A and O'Brien J L 2014 *Nat. Commun.* **5** 4213
[10] Quintino M T, Dong Q X X, Shimbo A, Soeda A and Murao M 2019 *Phys. Rev. Lett.* **123** 210502
[11] Cho S M, Kim A, Choi D, Choi B S and Seo S H 2020 *IEEE Access* **8** 213244
[12] Blunt N S, Caune L, Izsák R, Campbell E T and Holzmann N 2023 *PRX Quantum* **4** 040341
[13] Chen Z L, Guan Z J, Zhao S X and Chen X Y 2025 *Chin. Phys. B* **34** 050305
[14] Yang Z P, Zhang Y R, Li F L and Fan H 2024 *Chin. Phys. B* **33** 090304
[15] Russo A E, Rudinger K M, Morrison B C A and Baczewski A D 2021 *Phys. Rev. Lett.* **126** 210501
[16] Matsuzaki Y, Hakoshima H, Sugisaki K, Seki Y and Kawabata S 2021 *Jpn. J. Appl. Phys.* **60** SBBI02
[17] Fan J J, Ou Z Y and Zhang Z D 2024 *Light Sci. Appl.* **13** 163
[18] Liu M, Zhu J Y, Zhao G H, Li Y X, Yang Y P, Gao K M and Wu K F 2025 *Nat. Mater.* **24** 260
[19] Motta M, Sun C, Tan A T K, O'Rourke M J, Ye E, Minnich A J, Brandão F G S L and Chan G K L 2020 *Nat. Phys.* **16** 205
[20] Preskill J 2018 *Quantum* **2** 79
[21] Griffiths R B and Niu C S 1996 *Phys. Rev. Lett.* **76** 3228
[22] Li J X 2024 *Phys. Rev. A* **109** 032606
[23] Paesani S, Gentile A A, Santagati R, Wang J, Wiebe N, Tew D P, O'Brien J L and Thompson M G 2017 *Phys. Rev. Lett.* **118** 100503
[24] Smith J G, Barnes C H W and Arvidsson-Shukur D R M 2024 *Phys. Rev. A* **109** 042412
[25] Yamamoto K, Duffield S, Kikuchi Y and Ramo D M 2024 *Phys. Rev. Res.* **6** 013221
[26] Dobšíček M, Johansson G, Shumeiko V and Wendin G 2007 *Phys. Rev. A* **76** 030306
[27] Wiebe N and Granade C 2016 *Phys. Rev. Lett.* **117** 010503
[28] Sugisaki K, Sakai C, Toyota K, Sato K, Shiomi D and Takui T 2021 *Phys. Chem. Chem. Phys.* **23** 20152
[29] O'Malley P J J, Babbush R, Kivlichan I D, *et al.* 2016 *Phys. Rev. X* **6** 031007
[30] Santagati R, Wang J W, Gentile A A, *et al.* 2018 *Sci. Adv.* **4** eaap9646
[31] Nagata T, Okamoto R, O'Brien J L, Sasaki K and Takeuchi S 2007 *Science* **316** 726
[32] Slussarenko S, Weston M M, Chrzanowski H M, Shalm L K, Verma V B, Nam S W and Pryde G F 2017 *Nat. Photonics* **11** 700
[33] Pezzé L and Smerzi A 2009 *Phys. Rev. Lett.* **102** 100401
[34] Nielsen J A H, Neergaard-Nielsen J S, Gehring T and Andersen U L 2023 *Phys. Rev. Lett.* **130** 123603